

Relativistic Resonant Relations between Massive Black Hole Binary and Extreme Mass Ratio Inspiral

Naoki Seto

Department of Physics, Kyoto University Kyoto 606-8502, Japan

(Dated: December 16, 2018)

One component of a massive black hole binary (MBHB) might capture a small third body, and then a hierarchical, inclined triple system would be formed. With the post-Newtonian approximation including radiation reaction, we analyzed the evolution of the triple initially with small eccentricities. We found that an essentially new resonant relation could arise in the triple system. Here relativistic effects are crucial. Relativistic resonances, including the new one, stably work even for an outer MBHB of comparable masses, and significantly change the orbit of the inner small body.

I. INTRODUCTION

Merger of two massive black holes (MBHs) is one of the most violent events in the universe. A huge amount of energy is released in the form of gravitational waves (GWs). For a MBH binary (MBHB) with two masses $\sim 10^5$ - $10^6 M_\odot$, the Laser Interferometer Space Antenna [1] can easily detect the waves from virtually anywhere in the universe. Meanwhile, GWs from an extreme-mass-ratio inspiral [EMRI, more specifically, a compact object (*e.g.* neutron star, white dwarf) orbiting around a MBH] would enable us to closely examine gravitational theories using a map of the spacetime around the MBH, encoded in the waves [2, 3].

In a MBHB, either of MBHs might trap a small third object and form an EMRI (*e.g.* [4–6]). Such a compound triple system would be intriguing for cosmology and astrophysics. For example, with a tidal disruption of the small body, the MBHB merger could have precursive electromagnetic-wave signals that might allow us to identify the host galaxy of the MBHB and its redshift. Then we could observationally constrain the dark energy, using the luminosity distance estimated from the measurement of strong GWs emitted by the MBHB [7].

In the past ~ 200 years, orbital resonances have been ubiquitously identified among planetary or satellite systems obeying Newtonian dynamics [8]. For example, the mutual stability of Pluto and Neptune is maintained by their 3:2 orbital periods around the Sun. Therefore, one might expect that orbital resonances can be an effectual mechanism to form a stable three-body system including two MBHs. Indeed, except for detailed points, it was found that the resonant relations similar to those known in planetary/satellite systems could set up relativistic triple systems evolving by emitting gravitational radiation (see *e.g.* [9] for first order resonances such as 2:1 and also [10] for co-orbital ones). As in the case of Newtonian systems, the mass ratio of a MBHB involved in these familiar and strong resonances should be much smaller than unity (typically $\lesssim O(10^{-2})$) [11]. However, from the viewpoint of gravitational wave astronomy, it is preferable that a MBHB of comparable masses can resonantly trap a small third body.

In this paper, we report that an essentially new resonant relation could arise in a compound EMRI/MBHB system and it would significantly change the orbit of the inner EMRI. Here, relativistic effects, and inclined, hierarchical orbital configuration of the triple are crucial. These would be naturally realized for an EMRI/MBHB system, and the new resonance is among the two strong relativistic ones that work even for outer MBHBs of comparable masses, unlike the observed planetary or satellite systems.

This paper is organized as follows; in §II we describe our numerical method and summarize basic notations. In §III we show a typical orbital evolution under the new resonant relation. §IV is devoted to studies on the resonance. We first examine analytically how and why the resonance appears in our simulations, and then provide results from systematic numerical analyses. We also discuss issues related to gravitational wave measurements. In §V, we roughly evaluate the expected capture rate of a small third body for a MBHB. §VI is a summary of this paper.

II. NUMERICAL METHOD

In this paper, we numerically study evolution of a triple system composed by a MBHB (masses $m_0 = (1 - q)M$ and $m_1 = qM$) and a small inner particle $m_2 (\ll M)$ orbiting around m_0 (see Fig.1). Here M is the total mass of the MBHB and q is its mass ratio. We assume that m_0 and m_1 are comparable. The two objects m_0 and m_2 can be regarded as an EMRI progressively perturbed by the outer body m_1 whose distance to m_0 shrinks due to gravitational radiation reaction. Below, we adopt the geometrical unit with $G = c = M = 1$, and do not include effects of spins.

For equations of motion of the triple, we use the ADM Hamiltonian at 2.5 post-Newtonian (PN) order (see *e.g.*

arXiv:1202.4761v1 [astro-ph.CO] 21 Feb 2012

[12, 13]) formally written by

$$H = H_N + H_1 + H_2 + H_{2.5}. \quad (1)$$

Here H_N , H_1 and H_2 are the Newtonian, the 1PN and the 2PN terms respectively. $H_{2.5}$ is the first dissipative term induced by gravitational radiation. The Hamiltonian H is originally given for the position variables \mathbf{r}_i ($i = 1, 2, 3$: suffix for the particles) and their conjugate momenta \mathbf{p}_i . But, instead of \mathbf{p}_i , we introduce new variables $\mathbf{s}_i \equiv \mathbf{p}_i/m_i$ and take appropriate partial derivatives

$$\dot{\mathbf{r}}_i = \frac{1}{m_i} \frac{\partial H}{\partial \mathbf{s}_i}, \quad \dot{\mathbf{s}}_i = -\frac{1}{m_i} \frac{\partial H}{\partial \mathbf{r}_i} \quad (2)$$

in order to improve accuracy at numerically integrating systems with large mass ratios (the dot $\dot{}$ representing a time derivative). This prescription enables us to safely analyze the system even in the limit $m_2 \rightarrow 0$. But the three bodies m_0, m_1 and m_2 are handled equivalently in the post-Newtonian framework without introducing approximations associated with $m_2 \ll m_0, m_1$. We numerically integrate the equations of motion using a fifth order Runge-Kutta method with an adaptive step size control (see [9] for details of the numerical method).

We set up the initial conditions (denoted with the suffix “s”) of the compound EMRI/MBHB system, as follows. First, for the outer MBHB, we put its semimajor axis at $a_{1s} > 300$ with the circular orbital velocity including the 1PN correction. We can realize a small initial eccentricity $e_{1s} = O(10^{-4})$. Next, for the inner EMRI, we inject the small particle m_2 at the distance $a_{2s} (\ll a_{1s})$ from the moving body m_0 , and set its relative velocity at the Newtonian circular velocity, to generate a small eccentricity (typically $e_{2s} = O(10^{-2})$). For simplicity, we mainly set the initial eccentricities $e_{1s} \ll 1$ and $e_{2s} \ll 1$. Actually, for a single MBH, a majority of EMRIs might originate from dissolutions of stellar mass binaries by the MBH [14], and later become $e_2 \ll 1$ due to radiation reaction. In §V we revisit issues related to the orbital parameters of the inner EMRIs. Meanwhile, assuming independent evolutions of EMRI/MBHB in earlier epoch, we randomly put their mutual orbital phase and inclination.

To monitor the orbital elements, we define the coordinate distances between the three particles as

$$d_1 \equiv d_{10} \equiv |\mathbf{r}_1 - \mathbf{r}_0|, \quad d_2 \equiv d_{20} \equiv |\mathbf{r}_2 - \mathbf{r}_0|, \quad d_{12} \equiv |\mathbf{r}_1 - \mathbf{r}_2|. \quad (3)$$

For $i = 1, 2$, the semimajor axis a_i and eccentricity e_i (including the forced ones) are calculated from the distance d_i through its consecutive maximum ($a_i(1 + e_i)$) and minimum ($a_i(1 - e_i) \equiv r_{pi}$: pericenter distance). The MBHB evolves predominantly by its gravitational radiation alone, and we have $a_1 \simeq d_1$ with $e_1 \sim e_{1s}(a_1/a_{1s})^{19/12} \ll 1$ [15]. Since we perturbatively include the relativistic effects, we terminate our numerical integration when the distance d_{ij} between any pair i - j becomes less than 10 times $m_i + m_j$ (either C1: $d_1 < 10M$ or C2: $d_2 < 10m_0$ or C3: $d_{12} < 10m_1$).

To define the angular variables of the inner and outer orbits, we introduce the Cartesian frame XYZ around the central body m_0 with fixed spatial directions (see Fig.1). Here the XY -plane is identical to the initial orbital plane of the MBHB. Because of the initial inclination of the EMRI, the orbital plane of the MBHB slightly precesses. However, given $m_0, m_1 \gg m_2$, the outer body m_1 virtually stays on the XY plane, and we use λ_1 for its angular position. Following standard conventions [8], we also define Ω_2 and ϖ_2 for the ascending node and the pericenter of m_2 . The inclination I_2 is the angle between the angular momentum of m_2 and the Z -axis.

To clarify the relative position between m_1 and m_2 , we also introduce a complimentary frame $X_R Y_R Z_R$ that is corotating with m_1 . The rotating X_R -axis is oriented from m_0 toward m_1 , and the Z_R -axis coincides with the original Z -axis. The coordinate values in the two frames are related by $\mathbf{X}_R = \mathbf{R}_Z(-\lambda_1)\mathbf{X}$. Here $\mathbf{R}_Z(-\lambda_1)$ represents the 3×3 rotation matrix around the Z -axis with the angle $-\lambda_1$ (and so on below).

For reference, we provide useful expressions for a binary with masses m and m' , semimajor axis a , and the eccentricity e . The Kepler angular frequency n , the relativistic apsidal precession rate $\dot{\varpi}_R$ by the 1PN term [16] are given by

$$n = \left\{ \frac{m + m'}{a^3} \right\}^{1/2}, \quad \dot{\varpi}_R = \frac{3n(m + m')}{a(1 - e^2)}. \quad (4)$$

Meanwhile, the orbital parameters a and e decay due to gravitational radiation reaction as [15]

$$\frac{-a}{\dot{a}} = \frac{5a^4(1 - e^2)^{7/2}}{64(m + m')mm'} \left(1 + \frac{73e^2}{24} + \frac{37e^4}{96} \right)^{-1}, \quad (5)$$

$$\frac{-e}{\dot{e}} = \frac{5a^4(1 - e^2)^{5/2}}{304(m + m')mm'} \left(1 + \frac{121e^2}{304} \right)^{-1}. \quad (6)$$

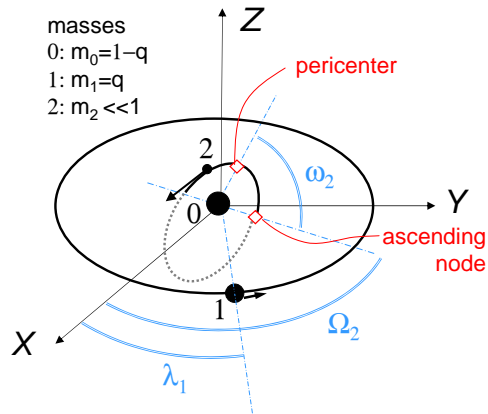


FIG. 1: Configuration of the compound EMRI/MBHB system. The XYZ -frame is defined around the central body m_0 , and its orientation is spatially fixed. The massive outer body m_1 virtually remains on the XY -plane (its initial orbital plane and used as our reference plane) with its angular position λ_1 . The inclined inner particle m_2 intersects with the XY -plane at the ascending node specified by Ω_2 . Its pericenter is described by the angle $\varpi_2 \equiv \Omega_2 + \omega_2$ (ω_2 : the angle between the ascending node and the pericenter). λ_2 , Ω_1 and ϖ_1 can be defined similarly, but less important in our study.

III. ORBITAL EVOLUTION

In Fig.2, we show the orbital elements of the inner EMRI in one of our runs. The three masses are $m_0 = 0.6$, $m_1 = 0.4$ and $m_2 = 10^{-6}$. We set the initial orbital parameters, $a_{1s} = 350$, $a_{2s} = 37m_0$, $I_{2s} = 74.3^\circ$, $e_{1s} \sim 10^{-4}$ and $e_{2s} \sim 3 \times 10^{-3}$. In Fig.2, we use the outer semimajor axis a_1 as an effective time variable moving leftward from $a_1 = 350$ down to ~ 160 .

At first, the EMRI evolves almost independently on the distant massive body m_1 , and its orbital decay rate \dot{a}_2 is close to the analytical prediction (5). Then, at $a_1 \sim 290$, the eccentricity e_2 and the inclination I_2 start to increase rapidly. The orbit of the EMRI becomes retrograde at $a_1 \lesssim 240$. Our integration is ended at $a_1 \sim 160$ by the condition C2 ($a_2(1 - e_2) \simeq 6$), when the time before the merger of the MBHB is $\sim 5.4(M/10^6 M_\odot)\text{yr}$.

In Fig.2d, we plot the combination of the angular parameters (modulo 2π)

$$\varphi \equiv 3\lambda_1 - \varpi_2 - 2\Omega_2 \quad (7)$$

sampled at intervals. This key variable initially shows no structured pattern, but becomes localized around $\varphi \sim +0$ at $a_2 \lesssim 300$ (satisfying $|\dot{\varpi}_2| \gg |\dot{\Omega}_2|$). It is clear that the EMRI is now resonantly trapped by the MBHB. To the best knowledge of the author, this is a new resonant state never discussed in the literature. As we see later, relativistic effects and the inclined, hierarchical orbital configuration are the crucial elements to raise the resonance. We also find that, for $H = H_N$ (without the PN terms), the eccentricity e_2 of this highly inclined system is quickly increased by the Kozai process [17] (easily destroyed by the relativistic apsidal motion [18]) and the run is ended shortly by the condition C2.

The combination φ indicates that the pericenter of the inner particle m_2 has a simple geometrical relation to the position of the massive outer body m_1 . In Fig.3, we plot the snapshots of the pericenter and the position of m_2 around the epoch $a_1 \sim 265$. We use the corotating frame $X_R Y_R Z_R$, and the pericenter lies almost on a distinct one-dimensional structure. Indeed, the shape of the curve is roughly given by the simple analytical expression

$$\mathbf{X}_R(u) = a_2(1 - e_2)\mathbf{R}_Z(-u)\mathbf{R}_X(I_2) \begin{pmatrix} \cos[3u] \\ \sin[3u] \\ 0 \end{pmatrix} \quad (8)$$

parameterized by $u \sim \lambda_1 - \Omega_2 \sim (\varpi_2 - \Omega_2)/3$. Here the rotation $\mathbf{R}_X(I_2)$ represents the tilt due to the inclination and $\mathbf{R}_Z(-u)$ is for the conversion to the corotating frame. The rapid evolution of e_2 and I_2 in Fig.2 can be understood as accumulation of coherent interactions between EMRI-MBHB through the established resonance.

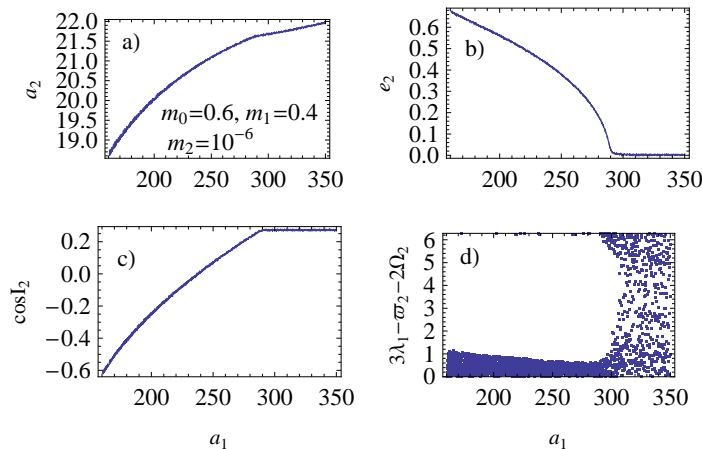


FIG. 2: Evolution of the inner EMRI, as a function of the decaying semimajor axis a_1 of the outer MBHB (leftward from $a_1 = 350$ down to 160). The panel (a) is for the inner semimajor axis a_2 . The inner eccentricity e_2 (panel b) and the inclination I_2 (panel c) show sudden changes around $a_2 \sim 290$ where the inner EMRI is resonantly captured by the outer MBHB, as shown in panel (d).

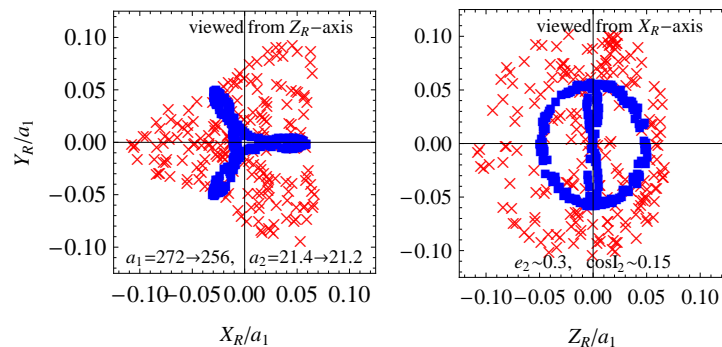


FIG. 3: The positions (crosses) and pericenters (filled squares) of the inner particle m_2 seen in the corotating $X_R Y_R Z_R$ -frame normalized by the outer distance a_1 . In this frame, the central body m_0 is at $(0, 0, 0)$ and the outer body m_1 is at $(1, 0, 0)$. The left panel is the projections of the points onto the $X_R Y_R$ -plane, and the right one onto the $Z_R Y_R$ -plane. These results are obtained from the same run as Fig.2. The points are sampled 200 times between $a_1 = 272$ and 256, corresponding to ~ 3400 orbital cycles of the outer MBHB. The pericenter of the EMRI is resonantly trapped by the MBHB, and stays nearly on the analytical curve (8) with $|\mathbf{X}_R| = a_2(1 - e_2)$.

IV. RESONANT MODES

A. Analytical Studies

Now, with the aid of the disturbing function, we discuss why the resonant variable φ appeared in our triple system. Roughly speaking, the disturbing function is a perturbative expansion of the effective gravitational potential between m_1 and m_2 both orbiting around a central body m_0 , and given by a summation of terms proportional to

$$\cos \left(\sum_{i=1}^2 j_i \lambda_i + k_i \varpi_i + l_i \Omega_i \right) \quad (9)$$

with integers j_i, k_i and l_i [8]. The disturbing function is usually applied for systems with $m_0 \gg m_1, m_2$ (e.g. planets around a star), but would prove to be quite useful to interpret our numerical results with $m_0 \sim m_1 \gg m_2$.

Since the outer MBHB continuously has $e_1 \ll 1$ and its orbital plane is almost unchanged, its pericenter and ascending node would not be important for the present resonant capture. Therefore, in the disturbing function, we

analyze the terms $A_{j_1 j_2 k l} \cos \phi_{j_1 j_2 k l}$ with the phases

$$\phi_{j_1 j_2 k l} \equiv j_1 \lambda_1 + j_2 \lambda_2 + k \varpi_2 + l \Omega_2. \quad (10)$$

Below, we assume $j_1 > 0$, as we are interested in explicit resonant couplings between EMRI-MBHB.

We rely on the three basic properties generally valid for the individual terms of the disturbing function [8, 19];

- (i) the sum rule; $j_1 + j_2 + k + l = 0$ from the rotational symmetry around the Z -axis,
- (ii) the scaling relation of the amplitude; $A_{j_1 j_2 k l} = O \left[e_2^{|k|} I_2^{|l|} (a_2/a_1)^p \right]$ for $e_2, I_2, (a_2/a_1) \ll 1$ with $p \geq 2$,
- (iii) the restriction of l to even numbers: $l = 2\nu$ (ν : integer) from the symmetry with respect to the XY -plane.

A resonant state is identified by the condition $\phi_{j_1 j_2 k l} \simeq \text{const}$. Here we analyze a more tractable form $\dot{\phi}_{j_1 j_2 k l} \sim 0$, and evaluate the magnitudes $(\dot{\lambda}_1, \dot{\lambda}_2, \dot{\varpi}_2, \dot{\Omega}_2)$ and the adequate integers (j_1, j_2, k, l) for the triple system with the hierarchy $a_2 \ll a_1$ and a small initial value $e_{2s} \ll 1$.

Because of the correspondence $\dot{\lambda}_i \sim n_i \propto a_i^{-3/2}$ (see eq.(4)) and the general relation $\dot{\lambda}_i \gg \dot{\varpi}_i, \dot{\Omega}_i$ valid also in weak field regime, our system satisfies $\dot{\lambda}_2 \gg \dot{\lambda}_1, \dot{\varpi}_2, \dot{\Omega}_2$. Then, for $j_2 \neq 0$, the condition $\dot{\phi}_{j_1 j_2 k l} \sim 0$ implies a very high-order resonance with $|j_1 + j_2| \sim |j_1| \sim |j_2|(a_1/a_2)^{3/2} \gg 1$. Instead, we limit our analysis only for the simpler cases with $j_2 = 0$.

Next we compare $\dot{\varpi}_2$ and $\dot{\Omega}_2$, by separately evaluating the secular Newtonian effects from the distant body m_1 and the relativistic effects around the nearby one m_0 . The Newtonian contributions $\dot{\varpi}_{N2}$ and $\dot{\Omega}_{N2}$ become $O(n_2(a_2/a_1)^3)$ [8], while the 1PN ones are $\dot{\varpi}_{R2} \sim 3n_2(1-q)/a_2$ (see eq.(4)) and $\dot{\Omega}_{R2} = 0$ [30]. The total relation becomes $\dot{\varpi}_2 \simeq \dot{\varpi}_{R2} \gg |\dot{\Omega}_2| \sim |\dot{\Omega}_{N2}|$, consistent with our numerical results. Thus, for our weak field system, the resonance $\varphi_{j_1 j_2 k l} \simeq \text{const}$ ($j_1 > 0$) should be realized with the relation $j_1 \dot{\lambda}_1 + k \dot{\varpi}_2 \sim 0$ ($k < 0$). Here, a smaller $|k|$ is preferred from the scaling relation (ii), and we put $k = -1$. In contrast, a small inclination angle $|I_2| \ll 1$ is not assumed, and we do not need to impose a strong requirement on $l = 2\nu$ at present. Then, the resonance variable valid for our system is written as

$$\theta_{;\nu} \equiv (2\nu + 1)\lambda_1 - \varpi_2 - 2\nu\Omega_2. \quad (11)$$

Below, we attach “;” before the mode-number suffixes ν to distinguish them from the labels i for the particles.

As seen so far, the relativistic effects are crucial to make $\dot{\theta}_{;\nu} \sim 0$ by increasing the apsidal precession rate $\dot{\varpi}_2$. In addition, the overall dissipative evolution is due to the 2.5PN radiation reaction force. At the resonance, the PN order parameter $(1-q)/a_2 = O(\dot{\varpi}_2/n_2)$ of the EMRI is comparable to the orbital hierarchy $(a_2/a_1)^{3/2} \sim n_1/n_2$. Thus, our sequence $\theta_{;\nu}$ contains only the outer position λ_1 without the inner one λ_2 , remarkably different from the standard mean motion resonances with $j_1 j_2 \neq 0$. Here, the unusually large outer mass $m_1 (\sim m_0)$ would enhance the resonant coupling.

The observed combination φ in eq.(7) is properly reproduced as $\varphi = \theta_{;1}$. Interestingly, for $\nu = 0$, the variable $\theta_{;0}$ coincides with the $j = 1$ inner Lindblad resonance. The Lindblad resonances [here parameterized by $j\lambda_1 - (j-1)\lambda_2 - \varpi_2$] play fundamental roles in the dynamics of coplanar disks [20] whose relativistic effects are recently discussed in [21].

From a basic relation of the disturbing function (*e.g.* eq.(12) in [19]), we get $p = \max\{3, 2\nu + 1\}$ for the relation (ii) with the variables $\theta_{;\nu}$. This shows weaker coupling for $\nu \geq 2$. Actually, even for $|k| = 2$, we have $p \leq 3$ only for $\phi = 2\lambda_1 - 2\varpi_2$ that completely degenerates with $\theta_{;0} = \lambda_1 - \varpi_2$.

In the C ring of Saturn, there is a ringlet structure whose longitude of the pericenter ϖ is in a resonant relation with the angular position λ_T of Titan, the largest satellite of Saturn. The resonant variable is given by $\lambda_T - \varpi$, and the apsidal precession $\dot{\varpi}$ of the ringlet is mainly caused by the large multipole moments of Saturn (*e.g.* its quadrupole moment $J_{20} = 0.016$) [22], instead of relativistic corrections.

Now we can predict when the inner EMRI with $e_2 \sim 0$ is resonantly captured by the outer MBHB. From the relation $(2\nu + 1)\dot{\lambda}_1 - \dot{\varpi}_2 \simeq 0$ (or equivalently $2\nu + 1 \simeq \dot{\varpi}_2 R/n_1$), the critical inner semimajor axis $\gamma_{;\nu}$ is given as a function of a_1 by

$$\gamma_{;\nu} = 3^{2/5} (2\nu + 1)^{-2/5} (1-q)^{3/5} a_1^{3/5}. \quad (12)$$

For $\nu = 0$ and the test particle limit $q = m_1 \rightarrow 0$, this expression coincides with eq.(130) in [21] for the $j = 1$ inner Lindblad resonance. Using the results in Fig.2, we also confirmed that the ratio $\dot{\varpi}_2/n_1 \propto a_1^{3/2} a_2^{-5/2}/(1-e_2^2)$ is nearly constant during the trapping.

B. Numerical Studies

Next we systematically analyze a series of numerical simulations. We take the mass parameters; $q = 0.4$, $m_2 = 10^{-6}$ and the initial conditions; $e_{1s} < 10^{-4}$, $e_{2s} < 10^{-2}$, $a_{1s} = 350$. We prepared totally 11 runs from various initial inner

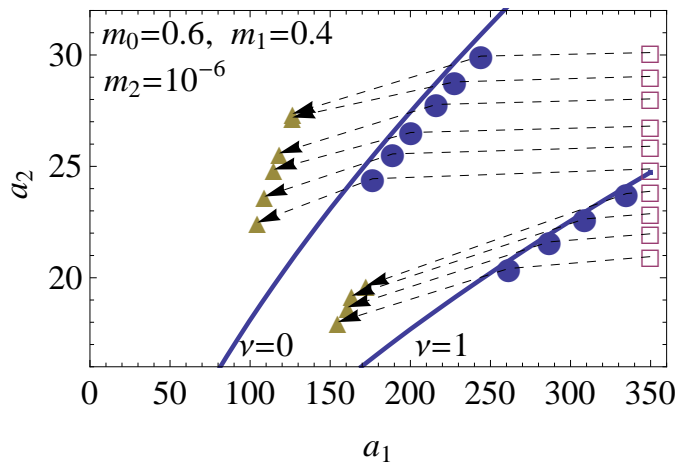


FIG. 4: Evolution of the triple systems in the a_1a_2 -plane. The open squares are the initial conditions with $a_{1s} = 350$ and $a_{2s} = 20-30$. The circles represent the points when e_2 exceeded 0.1 (indicating resonant capture), and the triangles are the termination points of the runs (all by the condition C2). The two solid curves are the analytical predictions (12) for the onsets of the resonant capture for $\nu = 1$ and 0.

separations $a_{2s} \in [33.3m_0, 50m_0]$ with random initial inclinations $\cos I_{2s} \in [0, 1]$. For these sets (a_{1s}, a_{2s}) , the infall rate is larger for the MBHB (namely $d(a_2/a_1)dt > 0$). From eq.(5), this catch-up condition is written as $a_2 > \eta_c a_1$ with $\eta_c \equiv (m_0 m_2 / m_1 M)^{1/4}$. When we reverse the time, each non-resonant triple moves on the curve

$$a_2^4 - (\eta_c a_1)^4 = \text{const} \quad (13)$$

and asymptotically approaches to the line $a_2 = \eta_c a_1$.

In Fig.4, we provide the time evolutions of the runs. We obtained similar results without the 2PN term. The run from $a_{2s} \simeq 22$ is what was already shown in Fig.2. In Fig.4 we added the analytical predictions $a_2 = \gamma_{;\nu}$ ($\nu = 0, 1$) for the onset of the resonant capture. They reasonably agree with the numerical results. Since the initial outer distance $a_{1s} = 350$ is not sufficiently large for $a_{2s} \gtrsim 25$, the corresponding EMRIs are captured by the $\nu = 0$ mode. We also examined dependence of the resonant captures on the mutual inclination of the two orbits. It was found that slightly inclined EMRIs (*e.g.* $I_{2s} = 0.14$ and 0) could pass through the $\nu = 1$ mode and first reacted to the $\nu = 0$ mode, in accord with the scaling relation $A_{j_1 j_2 k l} \propto (I_2)^{2\nu}$.

We briefly describe other interesting results. First, to realize a capture, the resonant curve $a_2 = \gamma_{;\nu}$ ($\nu = 1, 0$) in Fig.4 should be encountered in the direction $\dot{\nu} < 0$. For $\dot{\nu} > 0$, both e_2 and I_2 show gaps at the resonant crossings, but the capture was unsuccessful. Using eq.(12) in the form $(2\nu + 1) \propto a_1^{3/2} a_2^{-5/2}$, we can assign contour levels ν on the (a_1, a_2) plane. Then, from eq.(5), we obtain

$$\text{sign}(\dot{\nu}) = \text{sign}\left(\frac{3}{5} \frac{\dot{a}_1}{a_1} - \frac{\dot{a}_2}{a_2}\right) = \text{sign}(\kappa \eta_c a_1 - a_2) \quad (14)$$

with $\kappa \equiv (5/3)^{1/4}$. Therefore, we have $\dot{\nu} < 0$ (required for captures) at $a_2 > \kappa \eta_c a_1$. In Fig.5, we provide a schematic illustration for the resonant capture. We denote the intersection of the line $a_2 = \kappa \eta_c a_1$ with the resonant curve $a_2 = \gamma_{;\nu}$ by $(x_{1;\nu}, x_{2;\nu})$. For a capture by the ν mode, a triple should cross its resonant curve at $a_1 < x_{1;\nu}$ (the solid part in Fig.5). Furthermore, as understood from the flows of triples in the (a_1, a_2) -plane, an EMRI capturable either by $\nu = 0$ or 1 must exist in $\kappa^{-1} x_{2;0} < a_2 < x_{2;0}$ (shown by the double line in Fig.5) at the critical epoch $a_1 = x_{1;0}$.

Secondly, for the parameters shown in Fig.2, we examined systems with larger e_{2s} . For $e_2 \gtrsim 0.11$, the system transversed the $\nu = 1$ curve without a capture but again showed gaps of e_2 and I_2 . In the same manner, we analyzed the crossing of the $\nu = 0$ mode around $a_1 \simeq 200$ and $a_2 \simeq 29$ with various eccentricities e_2 , and found an upper limit $e_2 \sim 0.35$ for yielding captures. Similar behaviours (e_2 - or $\text{sign}(\dot{\nu})$ -dependence of the captures, observed gaps of e_2 at the resonant crossings without captures) are found for standard mean motion resonances and well explained by the separatrix structure in an effective phase space (see Figs.3-6 in [19] and also [23]).

By dropping the time consuming 2PN term, we also performed runs from $a_{1s} \sim 600$ and $a_{2s} \sim 30$ (corresponding to $\nu > 3$ in Fig.4). But the captures by the $\nu > 1$ modes did not occur, as anticipated from the arguments on the power p in the relation (ii). Furthermore, by artificially multiply a large factor to the dissipative term $H_{2.5}$, we evolved widely separated systems ($a_1 \sim 2000$ and $a_2 \gtrsim \gamma_0 \sim 100$ for $\nu = 0$) at accelerated rates, and confirmed captures by the $\nu = 0$ mode.

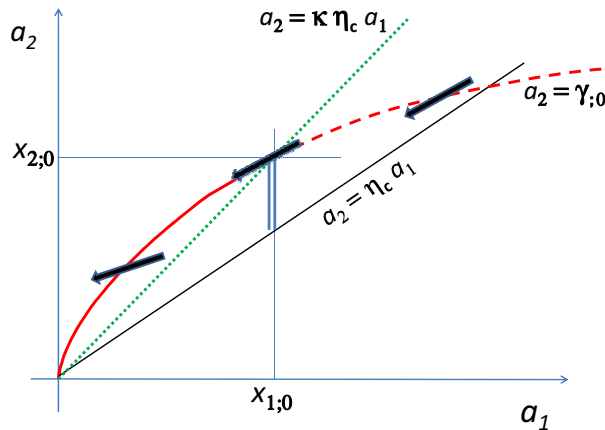


FIG. 5: Resonant capture of the inner EMRI by the outer MBHB. We show a schematic illustration for the $\nu = 0$ mode with a small eccentricity $e_2 \simeq 0$. The thick (solid and dashed) curve is the critical semimajor axis $a_2 = \gamma_{;0}$ of the EMRI for the resonant condition (12). The solid line $a_2 = \eta_c a_1$ is the catch-up line where we have $a_1^{-1} da_1/dt = a_2^{-1} da_2/dt$. The dotted line $a_2 = \kappa \eta_c a_1$ with $\kappa = (5/3)^{1/4}$ divides the signature of the resonance approach $\text{sign}(\dot{\nu})$, as shown by the three arrows. We put the intersection of the two curves by $(x_{1;0}, x_{2;0})$. To realize a capture, the resonant curve $a_2 = \gamma_{;0}$ should be crossed in the direction $\dot{\nu} < 0$, corresponding to the upper region of the dotted line (the solid part of the curve $a_2 = \gamma_{;0}$). Therefore, at the critical outer distance $a_1 = x_{1;0}$, the capturable inner EMRI must have a semimajor axis $\kappa^{-1} x_{2;0} < a_2 < x_{2;0}$ shown by the vertical double line.

C. Gravitational Wave Measurements

Here, we discuss GW detection for a trapped EMRI. In Fig.2, the final infall rate $\dot{r}_{p2} = d[a_2(1 - e_2)]/dt$ is ~ 70 times larger than that of a corresponding isolated EMRI (see eqs.(5) and (6)). Considering the effective time duration of the GW signals, the detectable distance for the trapped one becomes $\sim 1/\sqrt{70}$ times smaller. This is partly due to the small inner mass $m_2 = 10^{-6}$, and, indeed, the results in Fig.2 are similar to those for a test particle with $m_2 = 0$. We thus analyzed systems with larger m_2 from $(a_{1s}, a_{2s}) = (305, 21.5)$ now down to $r_{p2} = 6m_0$. The resonant trapping was successful up to $m_2 \sim 10^{-5}$ for which the trapping ended at $r_{p2} \sim 8m_0$ with the final rate \dot{r}_{p2} close to the isolated EMRI. But the corrections higher than 2.5PN could become important here.

To detect a trapped EMRI, a simple data analysis worth trying is a search triggered by strong GW of a merging MBHB that provides *e.g.* m_1, m_2 , the sky location of the system and also a_1 as a function of time. Here the primary orbital parameters of the EMRI would be its semimajor axis a_2 , eccentricity e_2 and mutual inclination I_2 . These should be searched by using templates. The trapping condition $a_1^{3/2} \propto a_2^{5/2}(1 - e_2^2)$ might become useful to narrow the parameter space of a_2 and e_2 to be surveyed.

Now we go back to the specific system shown in Fig.2, as an example, and discuss its final phase around $a_1 \sim 160$ and $a_2 \sim 19$. The orbital periods of the EMRI and the MBHB are ~ 700 and ~ 13000 respectively. Since the EMRI has a large eccentricity, it emits relatively strong pulse-like GWs around its pericenter. These GWs would be an interesting observational target. The characteristic duration of each pulse is $(r_{p2}^3/m_0)^{1/2} \sim 20$ and the interval between the adjacent pulses is approximately the orbital period of the EMRI. Therefore, the semimajor axis a_2 is the critical parameter for matching the GW signals.

For a standard mean motion resonance, the inner and outer semimajor axes are related through a simple linear relation between the two orbital periods. For example, we have $a_2/a_1 \simeq [j/(j+1)]^{2/3}$ for the first order resonance with the librating variable $j\lambda_2 - (j+1)\lambda_1 \sim \text{const}$ ($j \geq 1$: an integer). This kind of relation would be quite helpful to estimate evolution of the inner axis a_2 from the observed GW signals of the merged MBHB. However, our hierarchical resonances $\theta_{;\nu}$ do not explicitly depend on the angular position λ_2 of the trapped EMRI, and we cannot directly deduce the key parameter a_2 for the EMRI, as a function of a_1 . Therefore, for an EMRI trapped in our resonances, the identification of its GW signature could become more demanding, compared with standard mean motion resonances.

V. CAPTURE RATE

In this section, we roughly discuss probability of a MBHB ($2 \times 10^6 M_\odot + 10^6 M_\odot$) trapping a $10 M_\odot$ BH at the $\nu = 0$ and 1 modes. With respect to these mass parameters, the critical point in Fig.5 is given by

$$(x_{1;0}, x_{2;0}) = (2040, 118). \quad (15)$$

The formation scenario of an EMRI around a single MBH (not around a MBHB) often studied in the literature is the capture of a compact object around its close approach to the MBH by emission of gravitational radiation (hereafter two-body capture process) [24–26]. However, the formed EMRI would be highly eccentric, and the residual eccentricity has a typical value $e_2 \sim 0.5$ even when entering into the LISA band, corresponding to $a_2 = O(10)$ [25]. Therefore, considering the thresholds for the inner eccentricity e_2 discussed in §IV.B, the resonant capture by an outer MBHB would not be promising for the EMRIs formed by the two-body capture process.

Miller et al. [14] discussed formation of an EMRI through a tidal dissolution of a compact stellar binary by an MBH (hereafter binary dissolution process). One component of the binary is expelled from the system as a high-velocity star [27] and another one becomes bound to the MBH. The resultant EMRI could have a larger initial pericenter distance (thus a larger cross section for its formation), compared with the two-body capture process, and could have comparable or larger population. In addition, for the binary dissolution process, the residual eccentricity e_2 becomes small $e_2 \sim 0$ in the LISA band, due to a long-term dissipative evolution of the orbit with emitting gravitational radiation.

Here, following [14], we evaluate the orbital parameters of the inner EMRI formed by the binary dissolution process, simply assuming that the EMRI is affected by the secondary MBH solely through the $\nu = 0$ and 1 resonances.

We first consider only the evolution of the EMRI without taking into account the secondary MBH m_1 . A compact stellar binary with an orbital separation a_{bin} and mass $\sim m_2$ is dissolved by the primary MBH m_0 at the distance

$$d_{2,tide} \sim \left(\frac{3m_0}{m_2}\right)^{1/3} a_{bin} \sim 8.8 \left(\frac{m_0}{2 \times 10^6 M_\odot}\right)^{1/3} \left(\frac{m_2}{10 M_\odot}\right)^{-1/3} \left(\frac{a_{bin}}{0.1 \text{AU}}\right) \text{AU}, \quad (16)$$

where we put the fiducial parameter $a_{bin} = 0.1 \text{AU}$ given in [14]. We regard $d_{2,tide}$ as the initial pericenter distance of the EMRI and also use the typical value $e_2 \sim 0.98$ quoted in [14] for the initial eccentricity.

Then, with eqs.(5) and (6), the merger time of the EMRI is given by $\sim 5 \times 10^9 \text{yr}$ (less than the age of the universe). At $a_2 = x_{2;0} = 118$, we have a significantly reduced eccentricity $e_2 \sim 0.17$ and the remaining time $1.1 \times 10^6 \text{yr}$ ($\propto a_2^4$). When the outer MBH inspirals down to the critical separation $a_1 = x_{1;0} = 2040$, the distribution of the inner EMRIs at $a_2 \leq x_{2;0}$ would be in a steady state, from our assumptions. We can characterize the distribution of the EMRIs by their infall rate at $R_{in} = 5 \times 10^{-8} \text{yr}^{-1}$ [24]. This rate R_{in} was originally given for the two-body capture process, but we use it for the binary dissolution process, following the arguments in [14]. Finally, the probability of a MBHB merger with a trapped $10 M_\odot$ BH can be evaluated as

$$P = (5 \times 10^{-8} \text{yr}^{-1})(1.1 \times 10^6 \text{yr})(1 - 3/5) = 0.022, \quad (17)$$

corresponding to the expected number of EMRIs on the double line in Fig.5.

Actually, the above probability P contains the contribution of the EMRIs that would be captured by the $\nu = 1$ mode. These EMRIs pass close to the lower bound $a_2 = \kappa^{-1} a_{1;0} = 103.9$ on the double line. Since we have $x_{2;\nu} \propto 1/(2\nu + 1)$, the branching ratio of these modes is given by

$$1 - 3^{-4} : 3^{-4} = 80 : 1, \quad (18)$$

and dominated by the $\nu = 0$ mode. For inner EMRIs with white dwarfs or neutron stars of $m_2 \sim O(1 M_\odot)$, the merger times become larger than the age of the universe for the previous input parameters $a_{bin} = 0.1 \text{AU}$ and $e_2 = 0.98$. But, if we can assume small evolved eccentricities $e_2 \lesssim 0.2$ at $a_2 = x_{2;0}$ and the steady-state distributions normalized by $R_{in} = 5 \times 10^{-8} \text{yr}^{-1}$, the probabilities become $P = O(1)$ for these EMRIs.

Thus far, we have considered only an isolated three-body system in a simplified manner. In reality, a pre-existing EMRI might be destroyed by other stars (*e.g.* scattered from the secondary MBH). But, at the same time, the secondary MBH could highly enhance the capture rate of EMRIs R_{in} , at least, for those formed by the two-body capture process [4]. This is an interesting possibility and would be worth examined in the context of the binary dissolution process.

In ongoing or planned wide-field surveys for transient electromagnetic waves (see [28] for recent results), we might detect a tidal disruption event resonantly driven by a merging MBHB. For such a event, the signature of the orbital period of the MBHB might be found in the temporal structure of the emitted electromagnetic waves (see [29] for related discussions). Here, an MBH more massive than $\sim 10^6 M_\odot$ can directly swallow a white dwarf without a tidal disruption, and we need to consider a main sequence star in this mass regime.

VI. SUMMARY

Orbital resonances might be a potential mechanism to append a small body to an inspiraling MBHB, and to maintain the compound EMRI/MBHB system. Based on the post-Newtonian approximation, we numerically examined such hierarchical three body systems evolved by emitting gravitational radiation. For mutually inclined orbital configurations, we found a new resonant state with the librating variable $\theta_{;1} = 3\lambda_1 - \varpi_2 - 2\Omega_2$. This resonant state, together with another state $\theta_{;0} = \lambda_1 - \varpi_2$, works relatively strongly for the triple systems. Here the relativistic apsidal precession is essentially important, and the post-Newtonian parameter at the capture becomes comparable to the hierarchy of the two orbits $(a_2/a_1)^{3/2}$. In contrast to standard mean motion resonances known among planetary/satellite systems, these relativistic resonances can prevail even for outer MBHBs of comparable masses. During these resonances, the eccentricity and inclination of the inner EMRI increase almost monotonically, and its pericenter distance could go down blow ~ 5 Schwarzschild radii.

In order to realize a capture into the resonances, an inner EMRI cannot have a large eccentricity. Therefore, EMRIs formed through the familiar two-body capture process would be difficult to be involved in the resonances. In contrast, the binary dissolution process can produce mildly eccentric EMRIs at the spatial scale in interest, and these EMRIs might be resonantly trapped by inspiraling outer MBHBs.

The author would like to thank Takahiro Tanaka, Xian Chen and anonymous referees for helpful comments. This work was supported by JSPS grant 2074015.

-
- [1] P. L. Bender et al. LISA Pre-Phase A Report, 1998.
 - [2] F. D. Ryan, Phys. Rev. **D56**, 1845-1855 (1997).
 - [3] P. Amaro-Seoane et al. Class. Quant. Grav. **24**, 113 (2007).
 - [4] X. Chen et al. Astrophys. J. **729**, 13 (2011).
 - [5] C. Wegg and J. N. Bode, Astrophys. J. **738**, L18 (2011); N. Stone and A. Loeb, Mon. Not. Roy. Astron. Soc. **412**, 75 (2011).
 - [6] N. Yunes, et al. Phys. Rev. D **83**, 044030 (2011).
 - [7] B. F. Schutz, Nature **323**, 310 (1986); D. E. Holz and S. A. Hughes, Astrophys. J. **629**, 15 (2005).
 - [8] C. D. Murray and S. F. Dermott, *Solar System Dynamics* (Cambridge University Press, UK, 1999).
 - [9] N. Seto and T. Muto, Mon. Not. Roy. Astron. Soc. **415**, 3824 (2011).
 - [10] H. Asada, Phys. Rev. D **80**, 064021 (2009); N. Seto and T. Muto, Phys. Rev. D **81**, 103004 (2010); J. D. Schnittman, Astrophys. J. **724**, 39 (2010).
 - [11] B. Gladman, Icarus, 130, 159, (1994); A. T. Lee, E. W. Thommes, F. A. Rasio, Astrophys. J. **691**, 1684 (2009).
 - [12] P. Jaranowski, G. Schaefer, Phys. Rev. **D55**, 4712 (1997).
 - [13] C. O. Lousto and H. Nakano, Class. Quant. Grav. **25**, 195019 (2008); P. Galaviz and B. Bruegmann, Phys. Rev. D **83**, 084013 (2011); P. Galaviz, Phys. Rev. D **84**, 104038 (2011).
 - [14] M. C. Miller et al. Astrophys. J. **631**, L117 (2005).
 - [15] P. C. Peters, Phys. Rev. **136**, B1224 (1964).
 - [16] L. D. Landau and E. M. Lifshitz, *The Classical Theory of Fields* (Pergamon Press, Oxford, 1971).
 - [17] Y. Kozai, Astron. J. **67**, 591 (1962).
 - [18] M. Holman, J. Touma and S. Tremaine, Nature **386**, 254 (1997); O. Blaes, M. H. Lee and A. Socrates, Astrophys. J. **578**, 775 (2002).
 - [19] S. J. Peale, *Satellites*, 159, (1986).
 - [20] J. Binney and S. Tremaine, *Galactic Dynamics* (Princeton University Press, Princeton, 2008).
 - [21] C. M. Hirata, Mon. Not. Roy. Astron. Soc. **414**, 3212 (2011).
 - [22] C. Porco, et al. Icarus, 60, 1 (1984).
 - [23] J. Henrard and A. Lemaître, Celestial Mechanics, 30, 197, (1983); N. Borderies and P. Goldreich, Celestial Mechanics, 32, 127, (1984); A. C. Quillen, Mon. Not. Roy. Astron. Soc. **365**, 1367 (2006).
 - [24] M. Freitag, Astrophys. J. **583**, L21 (2003).
 - [25] C. Hopman and T. Alexander, Astrophys. J. **629**, 362 (2005).
 - [26] D. Merritt, T. Alexander, S. Mikkola and C. M. Will, Phys. Rev. D **84**, 044024 (2011).
 - [27] J. G. Hills, Nature **386**, 254 (1997); Q. Yu and S. Tremaine, Astrophys. J. **599**, 1129 (2003); W. R. Brown, M. J. Geller, S. J. Kenyon and M. J. Kurtz, Astrophys. J. **622**, L33 (2005).
 - [28] J. S. Bloom et al., Science **333**, 203 (2011); D. N. Burrows, et al., Nature **476**, 421 (2011); B. A. Zauderer, et al., Nature **476**, 425 (2011).
 - [29] F. K. Liu, S. Li and X. Chen, Astrophys. J. **706**, L133 (2009).
 - [30] If the MBHBs are spinning, Ω_2 precesses e.g. due to the spin-orbit coupling at 1.5PN order. But, considering the self-adapting nature of orbital resonances, the spin and also other higher PN effects would not qualitatively change our results at least for slowly rotating MBHBs.